The Roles of Betaine – Ester Analogues of 1-N-alkyl-3-N'-methyl Imidazolium Salts: As Amphotropic Ionic Liquid Crystals and Organogelators

ARTICLE *in* RSC ADVANCES · DECEMBER 2013

Impact Factor: 3.84 · DOI: 10.1039/C3RA43067G

RSC Advances

RSC Publishing

PAPER

View Article Online
View Journal

Cite this: DOI: 10.1039/c3ra43067g

The roles of betaine-ester analogues of 1-*N*-alkyl-3-*N*′-methyl imidazolium salts: as amphotropic ionic liquid crystals and organogelators†

Jing C. W. Tseng, Rohini Rondla, Padi Y. S. Su and Ivan J. B. Lin*

Received 19th June 2013
Accepted 9th October 2013

DOI: 10.1039/c3ra43067g

www.rsc.org/advances

Betaine-ester analogues of 1-*N*-alkyl-3-*N*′-methyl imidazolium salts exhibiting both thermotropic and lyotropic liquid crystal behaviors are reported. Two typical compounds, structurally determined by single crystal X-ray diffraction exhibit an interdigitated bilayer packing. These compounds are gelators, which form gels in a variety of organic solvents such as chloroform, methanol, ethanol, tetrahydrofuran, while also exhibiting a lamellar mesophase. Results from IR and variable-temperature ^{1}H NMR spectroscopy studies show that a trace amount of water (0.3–0.5% by volume) in $CHCl_3$ plays a crucial role for developing the H-bonded network during gel formation. Ag-NPs (~5–10 nm size) obtained from lyotropic LC solution and LC gel exhibit different morphologies ranging from spherical to truncated triangular plates.

Introduction

During the recent developments of ionic liquids (ILs) and ionic liquid crystals (ILCs), imidazolium (Im) salts have become a major class of materials with widespread applications in scientific and technological fields.[1] There are two reasons behind the interest in developing Im salts. Firstly, a valuable focus is concerning to improve the properties of ILs such as low melting point, thermal stability, wide potential window to apply for electrochemical applications,[1a,2] and further as reaction media,[2d,3] as carbene precursors,[4] as gelators,[5] and as nanoparticle stabilizers,[6] *etc.* Apart from this, there is a great concern associated with their ability as anisotropic ion conductive materials,[7] templates for the fabrication of nanoparticles,[6d,8] as antimicrobial agents,[9] and as organized reaction media or ordered solvents.[10]

Gels with three dimensional (3D) networks are a fascinating class of soft materials. When gels possess LC properties, are called LC gels, and can be classified into LC physical gels and LC chemical gels. LC physical gels comprise a 3D fibrous aggregation of low-molecular weight compounds, driven by non-covalent interactions such as π–π stacking, hydrogen-bonding.[11] The LC chemical gels comprise covalently bonded 3D polymer networks and are obtained by polymerization of LC or non-LC monomers in LCs. In the literature, LC physical gels composed of neutral molecules are widely studied, which could induce or enhance electro-optical, photochemical, electronic properties. Formation of gels with ImILs (ionogels) have been reported and widely used as templates for the synthesis of functional nanocomposites, nanoporous materials, electrolytic membranes, and luminescent gels, and also been used as an efficient system in drug delivery.[5,12] Unfortunately, little works have been focused on LC gels of Im salts.[13,14]

Most of the ImILs/ILCs developed till-date are 1-*N*-alkyl-3-*N*′-methyl Im cations associated with different anions.[1] Unfortunately less effort has been developed to the synthesis of functionalized ImILCs.[9,15] In the literature, there are several reports on betaine-ester functionalised ammonium and Im salts having one or two carbon atoms separating the ester group and ammonium nitrogen have been proved that they are cleavable, biodegradable and are used as soft drugs due to the hydrolytic sensitivity of the ester portion. Recently, two patents have been granted for betaine-ester analogues of Im salts for their use in personal care preparations and as biodegradable solvents for the chemical industry respectively.[16]

Thus, in order to explore the possible use of betaine-ester analogues of Im salts as soft functional materials, we have undertaken to study their role in LC properties, gelation ability and in the synthesis of silver nanoparticles (Ag-NPs). Here, we present the synthesis and LC properties of betaine-ester analogues of 1-*N*-alkyl-3-*N*′-methyl ImILCs; which display both thermotropic and lyotropic LC behavior. These

Department of Chemistry, National Dong Hwa University, Shoufeng, Hualien 974, Taiwan. E-mail: ijblin@mail.ndhu.edu.tw; Fax: +886-3-863-3570

† Electronic supplementary information (ESI) available: Instrumentation, synthesis and characterization details of Im salts, and the preparation method of Ag-NPs. Crystal data and structure refinement for [C_1, EC_{16}-Im]Br and [C_1, EC_{14}-Im]BF_4 (Tables S1 and S2). The ORTEP and crystal packing structures of [C_1, EC_{16}-Im]BF_4 (Fig. S1 and S2). POM, DSC, TGA PXRD, FE-SEM results and UV-vis-images (Fig. S3–S11), and schematic illustration of critical gel concentration of [C_1, EC_n-Im]X (X = Br^-, BF_4^- and PF_6^-) (Fig. S7). CCDC 942009 and 942010. For ESI and crystallographic data in CIF or other electronic format see DOI: 10.1039/c3ra43067g

salts show gelation ability in organic solvents. We also report the preparation of Ag-NPs in lyotropic LC solution as well as in LC gel.

Results and discussion

Synthesis

Scheme 1 Illustrates the betaine-ester functionalized 1-*N*-alkyl-3-*N*′-methyl imidazolium salts studied in this work and are denoted as [C_1, EC_n-Im]X (E = –CH_2COO–; n = 8, 10, 12, 14, and 16 for X = Br^-; n = 12, 14, and 16 for X = BF_4^- and PF_6^-). A literature procedure was used for the synthesis of these salts.[17] The characterization details, ^{1}H NMR, ^{13}C NMR, and elemental analysis are described in the ESI.†

Crystal structures

Well-formed single crystals of [C_1, EC_{16}-Im]Br and [C_1, EC_{16}-Im]-BF_4, were grown from DCM–ether solution. Details of the crystallographic data of these two compounds are given in Tables S1 and S2† respectively. [C_1, EC_{16}-Im]Br crystallized in $P2_1/c$ space group has a cation and an anion in the unit cell. The cation adopts a rod-shaped geometry and the ORTEP drawing of this compound is given in Fig. 1(a). The alkyl chain is not parallel to the imidazole plane; the angle between the imidazole core and alkyl chain is 135.5°. Packing diagram of this compound shows that molecules assemble in a head to tail fashion with interdigitated alkyl chains to form bilayer type lamellae with a layer distance of 21.8 Å (Fig. 1(b) and (c)). There is a close contact interaction between C=O···H19A*, and C=O*···H19A of neighbouring long alkyl chains, with the distance of 2.65 Å as shown in Fig. 1(d). The bromide anion forms four hydrogen bonds with four different Im cations (Fig. 1(e)). The ester C=O bond length found is *ca.* 1.182 (6) Å and the C–O bond length is about 1.339 (6) Å, are comparable to the previous report.[18]

[C_1, EC_{16}-Im]BF_4 crystallized in $P\bar{1}$ space group has two cations and two anions in the asymmetric unit. The ORTEP drawing of this compound is given in Fig. S1.† The alkyl chains are also not parallel to the imidazole plane and in each unit cell they are arranged with two different angles *i.e.*, 121.1° and 154.8°. The conformation and packing fashion are similar to that of [C_1, EC_{16}-Im]Br (Fig. S2(a) and (b)†). The *d*-spacing of 33.0 Å is longer than that of the Br^- analogue. Further, as shown in Fig. S2(c)† a set of C=O group participates in the H-bonding with imidazolium ring hydrogen (C=O3···H69*), and another set of C=O group with neighbouring methylene hydrogen (C=O6**···H67C*).†

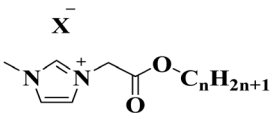

[C_1, EC_n-Im] X
E = -CH_2COO-
n = 8, 10, 12, 14, 16, and 18 for X^- = Br^-
n = 12, 14, and 16 for X^- = BF_4^- and PF_6^-

Scheme 1 Betaine-ester functionalized 1-*N*-alkyl-3-*N*′-methyl imidazolium salts prepared in this work.

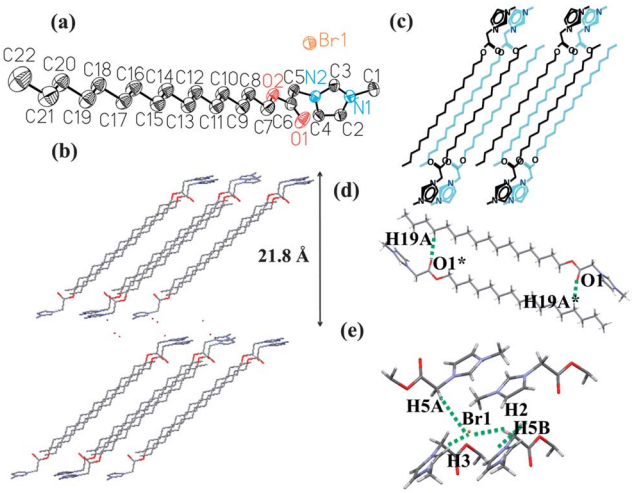

Fig. 1 (a) The ORTEP drawing structure of [C_1, EC_{16}-Im]Br (50% thermal ellipsoids), hydrogens being omitted for clarity; (b) crystal packing of [C_1, EC_{16}-Im]Br from *b* axis; (c) structure packing profile of [C_1, EC_{16}-Im]Br; (d) the hydrogen bonding *via* CH_2···O=C (O1*···H19A and O1···H19A*); O1* and H19A*: 2 − *x*, 1 − *y*, 2 − *z*. (e) H-bonding interactions around anion (Å): H5A···Br1: 2.69 Å; H5B···Br1: 3.05 Å; H2···Br1: 2.90 Å; H3···Br1: 2.65 Å. H5A: *x*, 1.5 − *y*, −1.5 + *z*; H5B: 1 − *x*, 1 − *y*, 2 − *z*; H2: *x*, *y*, −1 + *z*; H3: *x*, 1.5 − *y*, −1.5 + *z*.

Liquid-crystalline properties

Thermotropic liquid crystal (LC) properties of [C_1, EC_n-Im]X salts were studied by using polarized optical microscopy (POM), differential scanning calorimetry (DSC) and powder X-ray diffraction (PXRD). Using POM, all these salts exhibit fan-texture and often combined with homeotropic domains, therefore SmA mesophase is suggested. Typical POM images of [C_1, EC_{16}-Im]Br, [C_1, EC_{16}-Im]BF_4, and [C_1, EC_{16}-Im]PF_6 are shown in Fig. S3.†

The phase transition temperatures and enthalpy changes of all the compounds were determined by DSC from the second heating cycle and are summarized in Table 1. DSC traces for selective compounds in each series are included in the ESI (Fig. S4†). In the [C_1, EC_n-Im]Br series, compounds of n = 8, 10, and 12 are room temperature ionic liquid crystals (RTILCs) with melting points at <0 °C and clearing temperatures at 75.5, 138.2, and 188.6 °C, respectively. Compounds of n = 14, 16 and 18 show phase transition from crystal to mesophase at 82.3, 88.8 and 91.3 °C, and clearing processes at 228.2, 230.0 and 228.6 °C with partial decomposition. In the [C_1, EC_n-Im]BF_4^- series, salts with n = 12, 14, and 16 exhibit phase transition respectively from crystal to mesophase at 52.2, 63.2 and 72.8 °C and the transition to isotropic liquid at 164.1, 212.3 and 245.9 °C. In the [C_1, EC_n-Im]-PF_6 series, salts of n = 12, 14, and 16 show phase transition respectively from crystal to mesophase at 52.9, 62.2, and 69.8 °C, and the transition to isotropic liquid appears at 120.7, 168.7 °C and 205.2 °C. The decomposition temperatures were determined by thermogravimetric analysis (TGA) at a heating rate of 10 °C min^{-1} in inert (nitrogen) atmosphere. The BF_4^- and

Table 1 Phase transitions of the ester-functionalized imidazolium salts; [C_1, EC_n-Im]X (X = Br^-, BF_4^- and PF_6^-). The phase transition temperatures [°C] and enthalpies [kJ mol^{-1}] were determined from the second heating processes of DSC thermograms at a scan rate of 10.0 °C min^{-1}

Anion [X]	n	Temp. [°C]	ΔH [kJ mol^{-1}]	Phase transition[a]
X = Br^-	8	<0	—	SmA
		76	0.3	SmA → I
	10	<0	—	SmA
		137	0.6	SmA → I
	12	<0	—	SmA
		162	0.4	SmA → I
	14	82	34.3	Cr → SmA
		228	1.0	SmA → I[d]
	16	88.8	63.5	Cr → SmA
		230	0.8	SmA → I[d]
	18	66	9.0	Cr′ → Cr
		91	54.2	Cr → SmA
		229	0.5	SmA → I[d]
X = BF_4^-	12	52	36.0	Cr → SmA
		164	0.8	SmA → I
	14	63	44.9	Cr → SmA
		212	1.0	SmA → I
	16	73	59.5	Cr → SmA
		246	1.3	SmA → I
X = PF_6^-	12	53	42.8	Cr → SmA
		121	0.7	SmA → I
	14	62	40.3	Cr → SmA
		169	0.9	SmA → I
	16	70	48.5	Cr → SmA
		205	1.0	SmA → I

[a] Cr: crystal; SmA: smectic A; I: isotropic liquid; d: decompose.

PF_6^- salts show better thermal stability than the Br^- salts. The typical TGA curves for each series are shown in Fig. S5.†

In all series of salts, the melting and clearing points increase with increasing chain length presumably due to the enhanced van der Waals forces as has been proposal.[19] Counteranion also affects the LC property of these compounds. The melting points of Br^- salts are relatively higher than BF_4^- and PF_6^- salts possibly the stronger ionic and H-bonding interactions play the role. Salts of PF_6^- series have a much lower clearing temperatures and thus narrower mesophase ranges than those of the Br^- and BF_4^- series. This observation could be due to the week electrostatic interactions for the bulky PF_6^- as has been proposed.[20] However, all these Im salts show wider mesophase range than the reported 1-alkyl-3-methyl imidazolium salts; [C_1, C_n-Im]X (X = Br^-, BF_4^-, and PF_6^-).[21] This indicates that the ester functionality has profound effect in determining the mesophase stability, possibly due to a degree of polarizability by its π electrons associated with the carbonyl group.[22]

^{1}H NMR chemical shifts of these Im ring protons (C^2–H) clues the strength of the C^2–H···X coulombic interactions, which have a strong influence upon the mesophase stability.[21a,23] In order to suggest this result, at the same concentration, counteranion dependence of chemical shifts for the Im C^2–H proton is studied. The order of mesophase stability Br^- > BF_4^- > PF_6^- is same as the order of the strength of the C^2–H···X interactions. For example, for the [C_1, EC_{16}-Im]$^+$ cation, the chemical shift of C^2–H is 9.87 ppm for Br^-, 8.71 ppm for BF_4^-, and 8.54 ppm for PF_6^- anion. A gradual change from a down- to an up-field shift in going from Br^- to PF_6^- is observed as the size of the anion increased.[23b] This refers the weakening of H-bonding interactions for the bulky PF_6^- anion, and parallels the coulombic interaction strength.

Powder X-ray diffraction (PXRD) study was employed to characterize the mesophase structures of [C_1, EC_{16}-Im]X. At crystal phase, diffractograms show equally spaced peaks at small angle region indicating the lamellar structure. At mesophase a strong (100) reflection followed by weak (200), and (300) reflections at the small angle region, and a halo at the middle angle region are observed. For example, typical diffractograms for [C_1, EC_{16}-Im]-PF_6 at crystal phase and mesophase are shown in Fig. S6.† The d-spacing values for these salts are summarized in Table 2. In all salts, the increase of layer spacing from crystal phase at 30 °C to the mesophase at 120 °C suggest that the alignment of molecular rod perpendicular to the layer plane. The calculated long axes of mesogens (for example *ca.* 28 Å for [C_1, EC_{16}-Im]$^+$ cation) using Chem 3D software are significantly smaller than the experimental d-spacing in the mesophase, suggesting a bilayer arrangement (typically $L < d < 2L$ where L is the molecular length) with partial interdigitation of alkyl chains (Fig. 2).

Lyotropic liquid crystal (LLC) phases in $CHCl_3$

Formation of different lyotropic liquid crystal (LLC) phases at different concentrations of [C_1, EC_{16}-Im]Br in $CHCl_3$ is shown in Fig. 3. Below 16.1 wt% of the concentration, the solution is isotropic (Fig. 3(a)). At the concentration range of 16.1 to 21.9 wt %, the solution exhibits lamellar mesophase. The lamellar mesophase is supported by the observation of oily streak texture and homeotropic domain under POM (Fig. 3(b)). Further evidence comes from the diffractogram, which shows a sharp (100) peak followed by two weak (200), and (300) reflections (Fig. 3(e)). When the concentration is between 22.0 and 49.4 wt% (the maximum solubility), cubic mesophase is formed. The presence of cubic mesophase is confirmed by the typical homeotropic POM image shown in Fig. 3(c). Additionally, the diffractogram at 40 wt%, shows a sharp (200), and several weak (210), (211), (400), (331),

Table 2 The d-spacing of the betaine-ester functionalized Im salts

Anion [X^-]	n	d_{Cr}	d_{SmA}
X = Br^-	8	—	31.4[a]
	10	—	34.2[a]
	12	—	39.0[a]
	14	19.7[a]	36.6[b]
	16	21.3[a]	38.8[b]
	18	23.5[a]	44.4[b]
X = BF_4^-	12	28.3[a]	32.8[b]
	14	31.0[a]	35.6[b]
	16	33.5[a]	39.7[b]
X = PF_6^-	12	31.3[a]	33.1[b]
	14	33.5[a]	35.0[b]
	16	34.7[a]	37.6[b]

[a] At 30 °C. [b] At 120 °C.

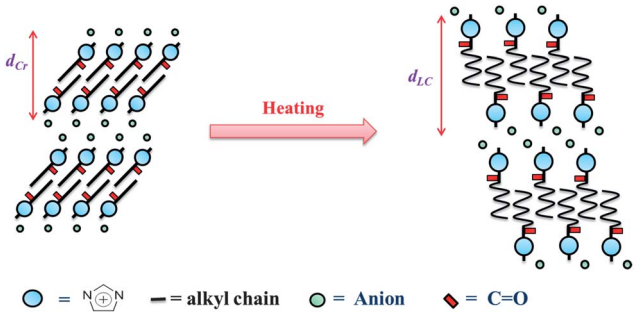

Fig. 2 Interdigitated bilayer molecular arrangement alterations of [C_1, EC_{16}-Im]X (X = Br^-, BF_4^- and PF_6^-) salts from solid state to mesophase.

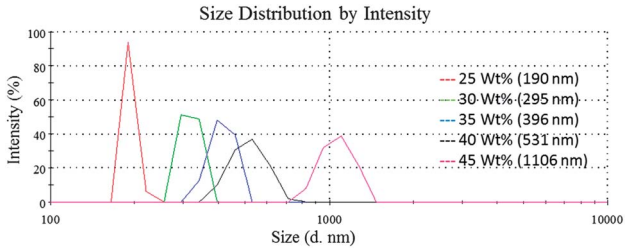

Fig. 4 Particles size distributions from DLS measurements of LLC cubic solution of [C_1, C_{16}-Im]Br in $CHCl_3$ with increase of concentrations.

(530), and (433) reflections suggesting the presence of inverse discontinuous micellar cubic phase ($Pm\bar{3}n$) (Fig. 3(f)).[24]

Dynamic light scattering (DLS) is a valuable tool for characterizing micelle or vesicle solutions, due to its sensitivity to particle size and polydispersity. Therefore, DLS study was used to determine the size of particles in the cubic solution of [C_1, C_{16}-Im]Br in $CHCl_3$ at different concentrations and the results are shown in Fig. 4. This illustrates the increase of particles size by increasing solution concentration. For example, the particle size is 190 nm in 25 wt% solution, and that increases to 295 nm, 396 nm, 531 nm, and up to 1106 nm in the 30 wt%, 35 wt%, 40 wt%, and 45 wt% solutions respectively. Usually, the size of small unilamellar vesicles (SUV) is <100 nm, and the size of large unilamellar vesicles (LUV) is 100–1000 nm, and the size of multi lamellar vesicles (MLV) is >1 μm.[25,26] Thus, we propose that LUV and MLV vesicles are formed in 25–40 wt% and 45 wt% of cubic solutions respectively. Fig. 4 better illustrates how the size distribution changes from monodispersed, large unilamellar vesicles to polydispersed, multilamellar vesicles *via* increasing concentration.

Optical microscopic images were also employed to follow the growth of particle sizes with increasing temperature for the 40 wt% cubic solutions. Results are shown in Fig. 5. At 35 °C, a mixture of spherical and ellipsoid vesicles with sizes of ~15 μm is noticed (Fig. 5(A)). Samples at 40 °C and 50 °C, show the aggregation of nearby vesicles to form clusters as shown in Fig. 5(B) and (C) respectively. The fusion of clusters into bulged vesicles with unfixed shape is seen at 55 °C as shown in image (D). Then through fission or leakage they form filament-like structure at 60 °C as shown in image (E). Vesicle is often flexible, so that the vesicle can easily change shape. The aggregation, fusion and fission are the most common processes in vesicles, and this can be induced by several stimuli such as temperature and osmotic pressure.[26] Probably, through heating, bulged vesicles could be disrupted to form filament like structures. Under these conditions, large sized MLV vesicles in the lyotropic cubic phase are no longer thermodynamically stable.

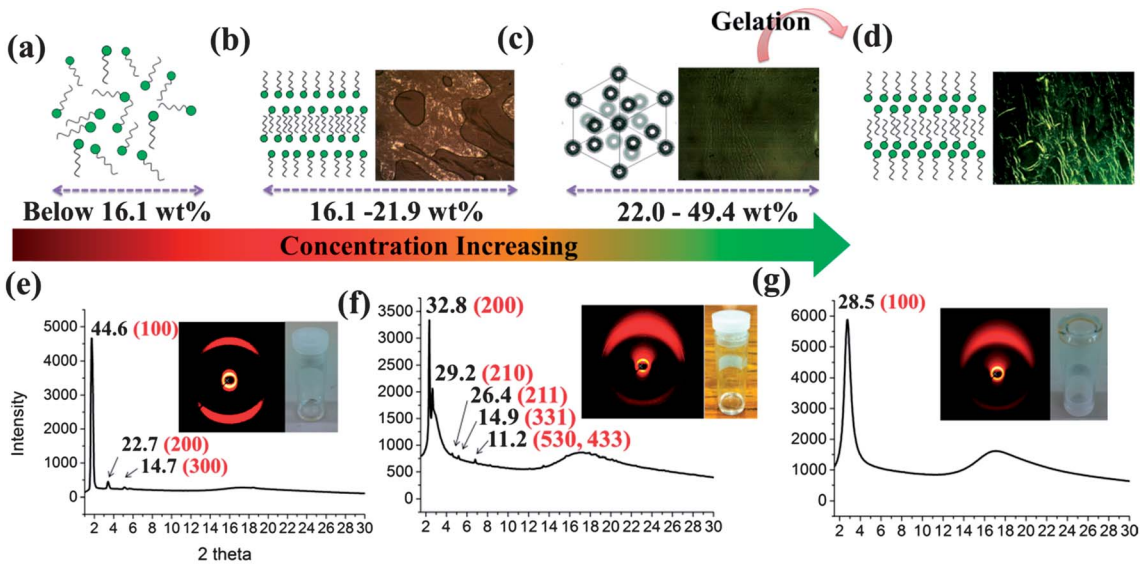

Fig. 3 (a) Schematic illustration of [C_1, EC_{16}-Im]Br salt isotropic state at below 16.1 wt%; and the POM and PXRD results of [C_1, EC_{16}-Im]Br salt in $CHCl_3$ solution at different salt gelling concentrations. (b and e) an oily streak POM image and X-ray diffraction pattern respectively indicating the lamellar mesophase at 18.0 wt%. (c and f) a homeotropic POM image at 22.0 wt% and X-ray diffraction pattern at 40.0 wt% respectively indicating discontinuous micellar cubic phase ($Pm\bar{3}n$) before gelation. (d and g) an oily streak and focal conic POM image at 22.0 wt% and X-ray diffraction pattern at 40.0 wt% respectively indicates the lamellar phase after gelation.

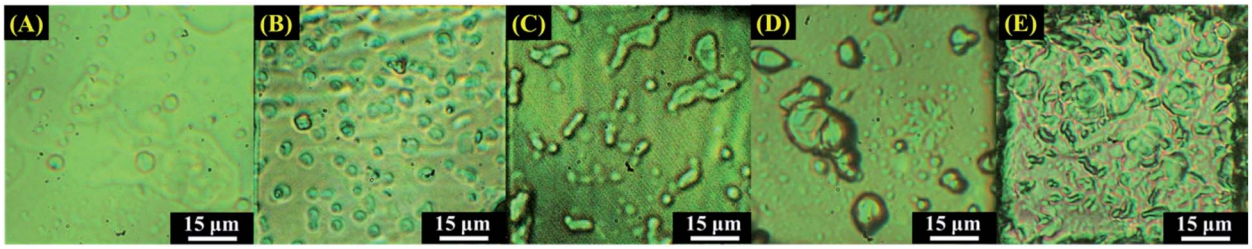

Fig. 5 Optical microscope images for 40 wt% cubic solution of [C_1, EC_{16}-Im]Br with $CHCl_3$ obtained without polarizer: (A) mixture of spherical and ellipsoid vesicles at 35 °C; (B) aggregation of vesicles at 40 °C; (C) clustering of vesicles at 50 °C; (D) merge or fusion into large clusters at 55 °C; (E) fission to form filaments at 60 °C.

Gelation study

These betaine-ester Im salts could form LC gel from organic solvents such as chloroform, dichloromethane, methanol, ethanol, and tetrahydrofuran. In the present investigation, chloroform ($CHCl_3$) is utilized as solvent for the gelation study. In the process of gelation, a $CHCl_3$ solution of [C_1, EC_{16}-Im]Br at 21.9–49.3 wt% concentration was heated up to 65 °C to get a clear solution, it was subsequently cooled to room temperature and rest for 5 h to obtain the gel. Gelation is a self-assembly process, as a common practice, a heating–cooling process could help to disperse the gelator in solution and develop the three dimensional framework throughout the solvent volume.[27] The heating–cooling cycle could in principle be repeated many times without affecting the gelation ability, suggest the gel obtained is thermally reversible. The gel exhibits no gravitational flow in inverted sample tube for several months (Fig. 6(a)). The gel-to-sol phase transition temperature (T_{gel}) is observed at 36.3 °C in the heating cycle by the technique of DSC (Fig. 6(b)). The gel exhibits lamellar mesophase as evidenced by the POM image showing focal-conic and oily streak (Fig. 3(d)), and by the diffractogram which exhibits one intense narrow low-angle (100) peak and a broad halo at near $2\theta = 8$, Fig. 3(g). In the heating–cooling cycle, the gel turns to isotropic solution at 36.3 °C, and the cubic phase disappeared; while cooling back to RT the lamellar gel remains. To our knowledge, no reports were found on the lyotropic LC phase transition before and after heating cooling cycle in the gelation process. Possibly, a simultaneous process of cubic solution to isotropic with filament MLV, followed by self-assembly into lamellar gel network occurring in the gelation process. However, the exact mechanism remains unclear.

Importantly, we could not observe any gel formation with dry $CHCl_3$. However, with a trace amount of water (0.3–0.5% by

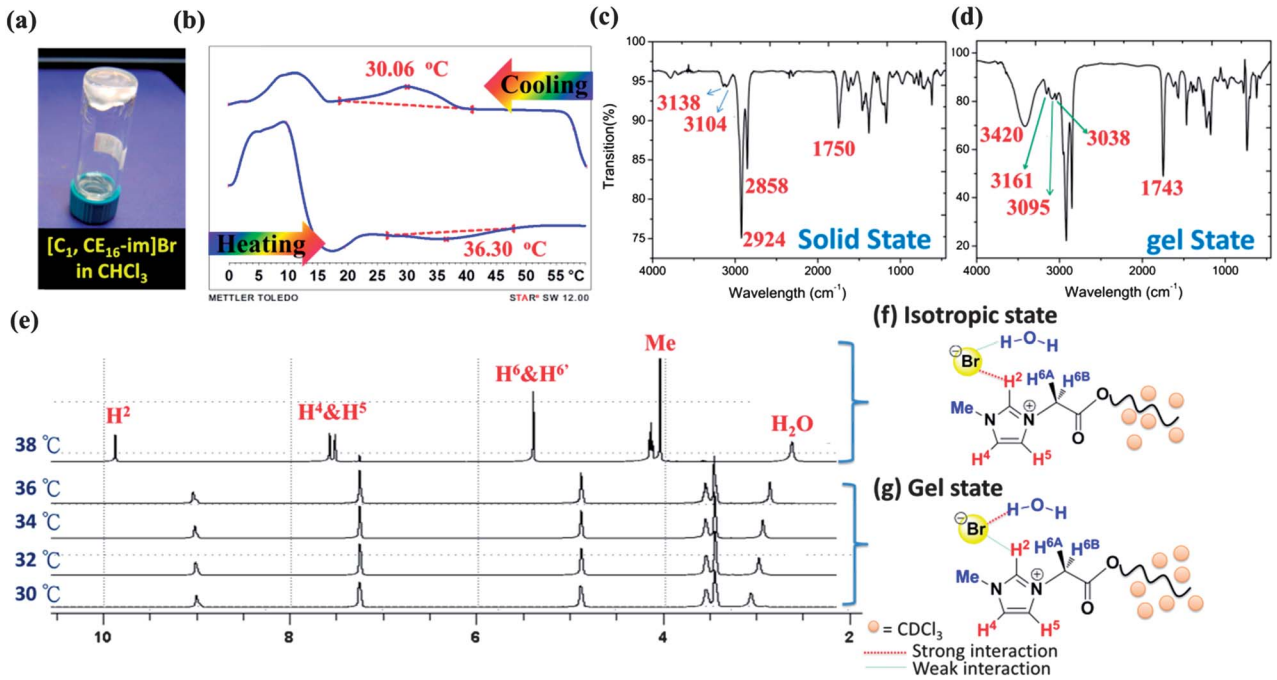

Fig. 6 (a) Viewing the stable gel state of [C_1, EC_{16}-Im]Br in $CHCl_3$ (45 wt%) towards the inversion of a sample vial; (b) DSC phase transition temperatures of the [C_1, EC_{16}-Im]Br gel; (c) IR spectra of [C_1, EC_{16}-Im]Br in gel state; (d) IR spectra of [C_1, EC_{16}-Im]Br in solid state; (e) variable-temperature ^{1}H NMR spectroscopy of the [C_1, EC_{16}-Im]Br in gel (30–36 °C) and isotropic (38 °C) state; and a schematic illustration for possible H-bonding interactions between C^2–H, Br^-, H_2O in solution state (f), and in gel state (g).

volume) in $CHCl_3$, gel could be formed. Thus, we can assume that, in our study, the traces of molecular water in the chloroform may participate in the formation of gel.[28,29] IR spectroscopy was utilized to elucidate the molecular interactions in the solid and gel states of [C_1, EC_{16}-Im]Br salt (Fig. 6(c)). Solid [C_1, EC_{16}-Im]Br shows two bands at 3104 cm^{-1} and 3138 cm^{-1}, which can be assigned to the Im ring sp^2 C–H stretching bands.[29] The ring sp^2 C–H vibrations in the gel state show three bands at 3161 cm^{-1}, 3095 cm^{-1} and 3038 cm^{-1}, presumably due to their reorganization of the H-bond network with Br^- anion and or water. This statement is supported by ^1H NMR results in the later discussion. The sp^3 C–H stretching bands of alkyl chain appear at 2858 cm^{-1} and 2924 cm^{-1} in the solid state, and at 2851 cm^{-1} and 2924 cm^{-1} in the gel state. This small variation may be due to the slight environmental changes of the C–H vibrations at N–CH_3 and alkyl chain. The carbonyl (C=O) stretching band appears at 1750 cm^{-1} in the solid state shifts to 1743 cm^{-1} in the gel state, possibly due to the slightly stronger C=O···H interactions during gel formation. The large band observed in the region of 3250 to 3600 cm^{-1} in the gel state is attributed to the stretching vibrations of water, which is absent in the solid state.

Variable-temperature ^1H NMR (VT-NMR) spectroscopy was also employed to study the gel of [C_1, EC_{16}-Im]Br in $CDCl_3$ to understand the phenomenon of molecular interactions. In the gel state (Fig. 6(e)), increasing the temperature from 30 to 36 °C there is a gradual down field shift for the C^2–H proton, but up field shift for H_2O. Upon further heating to 38 °C at which gel changes to solution state, a significant down field shift of the C^2–H proton from gel state (9.11 ppm at 36 °C) to solution (9.98 ppm at 38 °C) is observed. On the other hand, there is a greater up field shift observed for H_2O. These results suggest that the C^2–H proton is deshielded by the electronegative Br^- anion resulting from a stronger C^2–H···Br^- interaction in solution, yet a stronger H_2O···Br^- interaction in the gel. These findings are consistent with previous reports.[12j] Other protons (sp^2 $C^{4,5}$–H, sp^3 C^6–H, N–CH_3 and R–CH_3) are not influenced in the gel by increasing temperature, but shifted to down field from gel to solution, due to their local environment alterations. Based on the ^1H NMR and IR findings, we can assume that the H-bonded network comprising C^2–H···Br^-···H_2O, and C=O (ester carbonyl)···H_2O interactions are important in the formation of gel. Thus, indeed the trace amount of molecular water in $CHCl_3$ participates in the formation of gel.

Field-emission scanning electron microscopy (FE-SEM) was used to analyse the microstructure of xerogels obtained by air dry the gel overnight. The nanoflower microstructure appeared for the xerogel from [C_1, EC_{16}-Im]Br (Fig. 7(a)), specifies the absence of uniformly dispersed solvent in the void space.[30] Based on all experimental results, we can assume that the ease of gelation of these salts in $CHCl_3$ could be resulted by two main factors. Firstly, the formation of H-bond network comprising hydrophilic Im head group, ester functionality, molecular water, and Br^- anion. Secondly, the van der Waals interactions throughout the gel network *via* trapping $CHCl_3$ solvent molecules by hydrophobic alkyl chain region.[31]

The BF_4^- and PF_6^- salts in this study also exhibit LC gel behaviour in $CHCl_3$, albeit with higher critical gel concentration

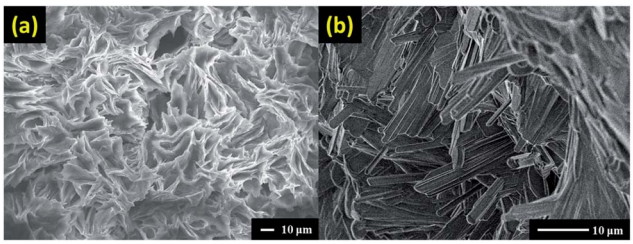

Fig. 7 FE-SEM images of dried samples of (a) xerogel of [C_1, EC_{16}-Im]Br and $CHCl_3$, (b) cubic solution of [C_1, EC_{16}-Im]Br and $CHCl_3$ before gelation.

than the Br^- series (Fig. S7†). The POM and PXRD results of these salts also show lamellar to cubic mesophase in the solution and lamellar phase in the gel state (see Fig. S8 and S9†). However, compared to the Br^- series, they show weaker gelation ability. The BF_4^- salt is found to be stable for about 2 months, while that of the PF_6^- salt is about one day. Possibly the large anionic size causes weaker coulombic and H-bonding interactions. A similar nanoflower morphology is observed for the [C_1, EC_{16}-Im]BF_4 and [C_1, EC_{16}-Im]PF_6 xerogels, and are shown in Fig. S10.† No fibrous network is observed from the micellar cubic solution of [C_1, EC_{16}-Im]Br and $CHCl_3$ before gelation (Fig. 7(b)), but instead rod like striped texture is found. This morphology implies the growth of crystal from solution rather than fibrous material, as has been reported previously.[32]

The previously reported [C_1, C_{10}-Im]X (X = Br^- and NO_3^-) salts are able to form lamellar LC gel in pure water,[12j] however, none of the present Im salts show gelation in pure water. This lack of hydrogelation is probably due to two factors. Firstly, these compounds are sparingly soluble in pure water, and secondly, the hydrolytic sensitivity of ester group leads a little extent of hydrolysis in deionized (DI) water at neutral pH 7, which is typical for betaine-ester surfactants.[16g,i] Dispersing the salt in DI water at RT, we also observe a lowering of pH value from 7 to 5.5 which further decreases to 2.7 after 1 day due to enhanced hydrolysis and then remain constant. This indicates that the Im salt is stable under these acidic conditions, which is a characteristic property for betaine-ester surfactants.[16g,i,k]

Preparation of silver nanoparticles (Ag-NPs)

Silver nanoparticles (Ag-NPs) were prepared from both the LLC solution and the LC gel of [C_1, EC_{16}-Im]Br in $CHCl_3$ *via* reduction of $AgNO_3$ by sodium borohydride ($NaBH_4$). A typical synthetic procedure is given in the ESI.† The morphology and size of Ag-NPs were examined by transmission electron microscopy (TEM). Ag-NPs obtained from LLC solution are spherical shape with diameters of 5–20 nm (Fig. 8(a)) and those from LC gel show mixed spherical and truncated triangular nanoplates of 5–10 nm sizes (Fig. 8(c)). Here, we can assume that in solution, the reduction process is rapid, therefore leads to a dominating spherical shaped NPs.[33] On the other hand, in the gel state the reduction process is slow and yields some anisotropic NPs. Probably, the decrease of diffusion rate from solution to gel state slows down the rate of reduction, nucleation, and growth. The ultraviolet-visible (UV-vis) spectrum for the solution sample (Fig. 8(b)), displays a single absorption

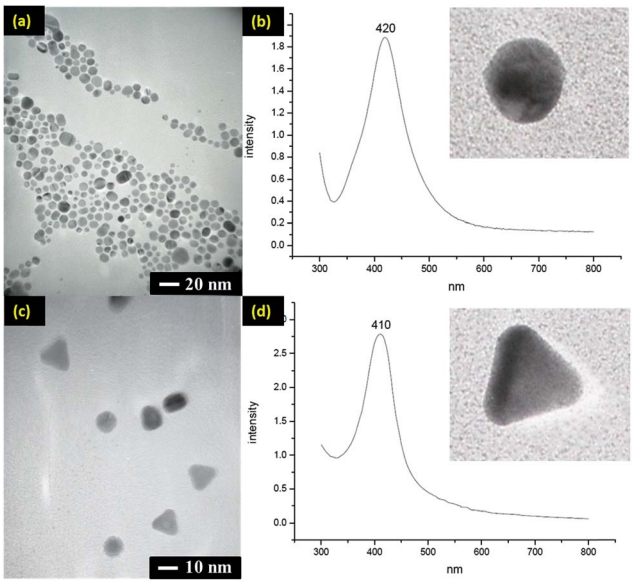

Fig. 8 The morphology of Ag-NPs prepared in LLC solution (a) and LC gel states of [C_1, EC_{16}-Im]Br/$CHCl_3$ (c) imaged by TEM, and their UV-bis images shown in (b) and (d) respectively.

band at 420 nm.[34] The gel sample spectrum displays an absorption band at 410 nm (Fig. 8(d)).[34a] The small blue shift of the absorption band observed from solution to gel sample is associated to the decrease in the size of NPs. These Ag-NPs in $CHCl_3$ solution are not stable under light, the yellow color; characteristic for Ag-NPs slowly disappears within 3 days. In dark, the yellow color slowly disappears for over one week, and the absorption peak experienced a red shift with decreased intensity (Fig. S11†), indicating the agglomeration of NPs. We also noticed that, the LC behavior still remains after vigorous stirring of $AgNO_3$ with LLC lamellar solution and LC gel samples, and alike for those subsequent Ag-NPs solutions. A confirmation for this comes from the analysis of broken fan like textures from POM and characteristic lamellar X-ray diffraction patterns for the same samples (Fig. S12†).

Conclusion

We have prepared a series of betaine-ester analogues of 1-*N*-alkyl-3-*N*′-methyl Im salts associating different anions and studied their thermotropic and lyotropic LC properties. These compounds show gelation ability in organic solvents but not in water. Interestingly, we notice that trace amount of water is necessary to form gel. Ag-NPs formed form LC solution or gel show different morphologies ranging from spherical to truncated triangular NPs. Betaine-esters analogues of Im salts are cleavable and biodegradable, and have been utilized for drug delivery as soft drugs. The additional properties presented here can be readily integrated with a wide range of technological and biological applications.

Acknowledgements

We thank the National Science Council (NSC) of Taiwan for financial support of this work. We thank the National Synchrotron Radiation Research Center of Taiwan and National Dong Hwa University Nano-Science and Technology Research Center (NSC 101-2120-M-259-002) for providing research facilities.

Notes and references

1 (*a*) D. D. Patel and J. M. Lee, *Chem. Rec.*, 2012, **12**, 329; (*b*) K. V. Axenov and S. Laschat, *Materials*, 2011, **4**, 206; (*c*) G. Singh and A. Kumar, *Indian J. Chem., Sect. A: Inorg., Bio-inorg., Phys., Theor. Anal. Chem.*, 2008, **47**, 495; (*d*) K. Binnemans, *Chem. Rev.*, 2005, **105**, 4148.

2 (*a*) V. Causin and G. Saielli, in *Green Solvents II: Properties and Applications of Ionic Liquids*, ed. A. Mohammad and Inamuddin, Springer, Dordrecht, Heidelberg, New York, London, 2012, ch. 4, pp. 79–118; (*b*) C. Badre, L. Marquant, A. M. Alsayed and L. A. Hough, *Adv. Funct. Mater.*, 2012, **22**, 2723; (*c*) M. Armand, F. Endres, D. R. MacFarlane, H. Ohno and B. Scrosati, *Nat. Mater.*, 2009, **8**, 621; (*d*) S. G. Lee, *Chem. Commun.*, 2006, 1049.

3 (*a*) J. P. Hallett and T. Welton, *Chem. Rev.*, 2011, **111**, 3508; (*b*) D. B. N. Allan and D. Headley, *Aldrichimica Acta*, 2007, **40**, 107.

4 L. A. Schaper, S. J. Hock, W. A. Herrmann and F. E. Kühn, *Angew. Chem., Int. Ed.*, 2013, **52**, 270.

5 (*a*) F. D'Anna, P. Vitale, S. Marullo and R. Noto, *Langmuir*, 2012, **28**, 10849; (*b*) J. Le Bideau, L. Viau and A. Vioux, *Chem. Soc. Rev.*, 2011, **40**, 907.

6 (*a*) M. A. Neouze, *J. Mater. Chem.*, 2010, **20**, 9593; (*b*) H. Chu, Y. Shen, L. Lin, X. Qin, G. Feng, Z. Lin, J. Wang, H. Liu and Y. Li, *Adv. Funct. Mater.*, 2010, **20**, 3747; (*c*) A. Imanishi, M. Tamura and S. Kuwabata, *Chem. Commun.*, 2009, 1775; (*d*) D. Batra, S. Seifert, L. M. Varela, A. C. Y. Liu and M. A. Firestone, *Adv. Funct. Mater.*, 2007, **17**, 1279.

7 (*a*) S. Yazaki, M. Funahashi, J. Kagimoto, H. Ohno and T. Kato, *J. Am. Chem. Soc.*, 2010, **132**, 7702; (*b*) S. Yazaki, M. Funahashi and T. Kato, *J. Am. Chem. Soc.*, 2008, **130**, 13206; (*c*) N. Yamanaka, R. Kawano, W. Kubo, N. Masaki, T. Kitamura, Y. Wada, M. Watanabe and S. Yanagida, *J. Phys. Chem. B*, 2007, **111**, 4763; (*d*) M. Yoshio, T. Kagata, K. Hoshino, T. Mukai, H. Ohno and T. Kato, *J. Am. Chem. Soc.*, 2006, **128**, 5570; (*e*) N. Yamanaka, R. Kawano, W. Kubo, T. Kitamura, Y. Wada, M. Watanabe and S. Yanagida, *Chem. Commun.*, 2005, 740; (*f*) M. Yoshio, T. Mukai, H. Ohno and T. Kato, *J. Am. Chem. Soc.*, 2004, **126**, 994.

8 (*a*) W. Dobbs, J. M. Suisse, L. Douce and R. Welter, *Angew. Chem., Int. Ed.*, 2006, **45**, 4179; (*b*) A. Taubert, P. Steiner and A. Mantion, *J. Phys. Chem. B*, 2005, **109**, 15542; (*c*) A. Taubert, *Angew. Chem., Int. Ed.*, 2004, **43**, 5380; (*d*) K. Binnemans, R. Van Deun, B. Thijs, I. Vanwelkenhuysen and I. Geuens, *Chem. Mater.*, 2004, **16**, 2021.

9 R. T. W. Huang, K. C. Peng, H. N. Shih, G. H. Lin, T. F. Chang, S. J. Hsu, T. S. T. Hsu and I. J. B. Lin, *Soft Matter*, 2011, **7**, 8392.

10 C. K. Lee, H. W. Huang and I. J. B. Lin, *Chem. Commun.*, 2000, 1911.

11 T. Kato, Y. Hirai, S. Nakaso and M. Moriyama, *Chem. Soc. Rev.*, 2007, **36**, 1857.

12 (*a*) J. Zhang and X. Shen, *J. Phys. Chem. B*, 2013, **117**, 1451; (*b*) T. Wen, H. Li, Y. Wang, L. Wang, W. Zhang and L. Zhang, *J.*

Mater. Chem. C, 2013, **1**, 1607; (*c*) S. S. Sekhon, D. P. Kaur, J. S. Park and K. Yamada, *Electrochim. Acta*, 2012, **60**, 366; (*d*) L. Viau, C. Tourne-Peteilh, J.-M. Devoisselle and A. Vioux, *Chem. Commun.*, 2010, **46**, 228; (*e*) J. C. Jansen, K. Friess, G. Clarizia, J. Schauer and P. Izák, *Macromolecules*, 2010, **44**, 39; (*f*) F. Gayet, L. Viau, F. Leroux, S. Monge, J. J. Robin and A. Vioux, *J. Mater. Chem.*, 2010, **20**, 9456; (*g*) Y. Zhao, X. Chen, B. Jing, X. Wang and F. Ma, *J. Phys. Chem. B*, 2009, **113**, 983; (*h*) K. Lunstroot, K. Driesen, P. Nockemann, C. Görller-Walrand, K. Binnemans, S. Bellayer, J. Le Bideau and A. Vioux, *Chem. Mater.*, 2006, **18**, 5711; (*i*) M. A. Firestone, M. L. Dietz, S. Seifert, S. Trasobares, D. J. Miller and N. J. Zaluzec, *Small*, 2005, **1**, 754; (*j*) M. A. Firestone, P. G. Rickert, S. Seifert and M. L. Dietz, *Inorg. Chim. Acta*, 2004, **357**, 3991.

13 N. M. Sangeetha and U. Maitra, *Chem. Soc. Rev.*, 2005, **34**, 821.

14 (*a*) T. Inoue, B. Dong and L. Q. Zheng, *J. Colloid Interface Sci.*, 2007, **307**, 578; (*b*) D. Batra, S. Seifert and M. A. Firestone, *Macromol. Chem. Phys.*, 2007, **208**, 1416; (*c*) D. Batra, D. N. T. Hay and M. A. Firestone, *Chem. Mater.*, 2007, **19**, 4423; (*d*) M. A. Firestone, J. A. Dzielawa, P. Zapol, L. A. Curtiss, S. Seifert and M. L. Dietz, *Langmuir*, 2002, **18**, 7258; (*e*) J. H. Davis Jr, K. J. Forrester and T. Merrigan, *Tetrahedron Lett.*, 1998, **39**, 8955.

15 (*a*) S. C. Luo, S. Sun, A. R. Deorukhkar, J.-T. Lu, A. Bhattacharyya and I. J. B. Lin, *J. Mater. Chem.*, 2011, **21**, 1866; (*b*) J. C. Y. Lin, C.-J. Huang, Y. T. Lee, K. M. Lee and I. J. B. Lin, *J. Mater. Chem.*, 2011, **21**, 8110; (*c*) P. H. J. Kouwer and T. M. Swager, *J. Am. Chem. Soc.*, 2007, **129**, 14042; (*d*) J. Y. Z. Chiou, J. N. Chen, J. S. Lei and I. J. B. Lin, *J. Mater. Chem.*, 2006, **16**, 2972; (*e*) K. M. Lee, Y. T. Lee and I. J. B. Lin, *J. Mater. Chem.*, 2003, **13**, 1079.

16 (*a*) J. Janiak, L. Piculell, K. Schillen and D. Lundberg, *Soft Matter*, 2013, **9**, 4103; (*b*) L. Mi, H. Xue, Y. Li and S. Jiang, *Adv. Funct. Mater.*, 2011, **21**, 4028; (*c*) S. Morrissey, B. Pegot, D. Coleman, M. T. Garcia, D. Ferguson, B. Quilty and N. Gathergood, *Green Chem.*, 2009, **11**, 475; (*d*) S. Morrissey, I. Beadham and N. Gathergood, *Green Chem.*, 2009, **11**, 466; (*e*) Y. Itoh and R. Akasaka, *J. Surfactants Deterg.*, 2009, **12**, 101; (*f*) J. R. Harjani, J. Farrell, M. T. Garcia, R. D. Singer and P. J. Scammells, *Green Chem.*, 2009, **11**, 821; (*g*) D. L. M. S. K. Holmberg, *Adv. Polym. Sci.*, 2008, **218**, 57; (*h*) R. M. C. S. Ramaa, A. S. Mundada and V. J. Kadam, *Indian J. Chem., Sect. B: Org. Chem. Incl. Med. Chem.*, 2008, **47**, 721; (*i*) D. Lundberg, M. Stjerndahl and K. Holmberg, *Langmuir*, 2005, **21**, 8658; (*j*) M. Stjerndahl, D. Lundberg and K. Holmberg, in *Surfactant Science Series, Novel Surfactants*, ed. K. Holmberg, Marcel Dekker, Inc., New York, USA, 2nd revised edition, 2005, vol. 114, p. 317; (*k*) P. E. Hellberg, K. Bergström and K. Holmberg, *J. Surfactants Deterg.*, 2000, **3**, 81; (*l*) B. Ahlström and L. Edebo, *Microbiology*, 1998, **144**, 2497; (*m*) K. Holmberg, *Curr. Opin. Colloid Interface Sci.*, 1996, **1**, 572; (*n*) S. A. M. Lindstedt, R. A. Thompson and L. Edebo, *Antimicrob. Agents Chemother.*, 1990, **34**, 1949; (*o*) W. V. Cohen and A. H. Corwin, *J. Am. Chem. Soc.*, 1953, **75**, 5880; (*p*) W. A. Farone and T. Palmer, *US Pat.* US 6,384,266 B1, 2002; (*q*) R. M. K. Dale and S. L. Gatton, *US Pat.* US 2005/0136458 A1, 2005; (*r*) M. T. Garcia, I. Ribosa, L. Perez, A. Manresa and F. Comelles, *Langmuir*, 2013, **29**, 2536; (*s*) S. T. Elder, A. Preuss, K. U. Schoning and K. Muhlbauer, *US Pat.* US 8,232,305 B2, 2012; (*t*) N. Gathergood, S. Morrissey and B. Pegot, *US Pat.* US 2011/0201824 A1, 2011.

17 S. Kanjilal, S. Sunitha, P. S. Reddy, K. P. Kumar, U. S. N. Murty and R. B. N. Prasad, *Eur. J. Lipid Sci. Technol.*, 2009, **111**, 941.

18 G. F. Starkulla, S. Klenk, M. Butschies, S. Tussetschlager and S. Laschat, *J. Mater. Chem.*, 2012, **22**, 21987.

19 K. M. Wiggins, R. L. Kerr, Z. Chen and C. W. Bielawski, *J. Mater. Chem.*, 2010, **20**, 5709.

20 (*a*) M. Yoshio, T. Ichikawa, H. Shimura, T. Kagata, A. Hamasaki, T. Mukai, H. Ohno and T. Kato, *Bull. Chem. Soc. Jpn.*, 2007, **80**, 1836; (*b*) G. A. Knight and B. D. Shaw, *J. Chem. Soc.*, 1938, 682.

21 (*a*) A. E. Bradley, C. Hardacre, J. D. Holbrey, S. Johnston, S. E. J. McMath and M. Nieuwenhuyzen, *Chem. Mater.*, 2002, **14**, 629; (*b*) J. D. Holbrey and K. R. Seddon, *J. Chem. Soc., Dalton Trans.*, 1999, 2133; (*c*) C. M. Gordon, J. D. Holbrey, A. R. Kennedy and K. R. Seddon, *J. Mater. Chem.*, 1998, **8**, 2627.

22 D. A. Dunmur and S. Singh, *Liquid Crystals: Fundamentals* (E-Book), World Scientific Pub. Co., Inc., 2002, ch. 4, p. 92.

23 (*a*) I. Sanchez, J. A. Campo, J. V. Heras, M. Rosario Torres and M. Cano, *J. Mater. Chem.*, 2012, **22**, 13239; (*b*) W. Dobbs, L. Douce, L. Allouche, A. Louati, F. Malbosc and R. Welter, *New J. Chem.*, 2006, **30**, 528; (*c*) K. M. Lee, C. K. Lee and I. J. B. Lin, *Chem. Commun.*, 1997, 899.

24 (*a*) H. Delacroix, T. Gulik-Krzywicki, P. Mariani and V. Luzzati, *J. Mol. Biol.*, 1993, **229**, 526; (*b*) P. Sakya, J. M. Seddon, R. H. Templer, R. J. Mirkin and G. J. T. Tiddy, *Langmuir*, 1997, **13**, 3706; (*c*) D. V. Perroni and M. K. Mahanthappa, *Soft Matter*, 2013, **9**, 7919.

25 J. H. Lee, V. Agarwal, A. Bose, G. F. Payne and S. R. Raghavan, *Phys. Rev. Lett.*, 2006, **96**, 048102.

26 J. Voskuhl and B. J. Ravoo, *Chem. Soc. Rev.*, 2009, **38**, 495.

27 Y. C. Lin, B. Kachar and R. G. Weiss, *J. Am. Chem. Soc.*, 1989, **111**, 5542.

28 (*a*) B. C. Bricknell, T. A. Ford and T. M. Letcher, *Spectrochim. Acta, Part A*, 1997, **53**, 299; (*b*) L. Cammarata, S. G. Kazarian, P. A. Salter and T. Welton, *Phys. Chem. Chem. Phys.*, 2001, **3**, 5192.

29 T. Wang, H. Kaper, M. Antonietti and B. Smarsly, *Langmuir*, 2007, **23**, 1489.

30 A. Sein, J. A. Verheij and W. G. M. Agterof, *J. Colloid Interface Sci.*, 2002, **249**, 412.

31 (*a*) G. Némethy, *Angew. Chem., Int. Ed.*, 1967, **6**, 195; (*b*) C. Tanford, *Science*, 1978, **200**, 1012.

32 T. Ban, H. Mitaku, C. Suzuki, J. Matsuba, Y. Ohya and Y. Takahashi, *J. Cryst. Growth*, 2005, **274**, 594.

33 X. Dong, X. Ji, J. Jing, M. Li, J. Li and W. Yang, *J. Phys. Chem. C*, 2010, **114**, 2070.

34 (*a*) M. E. Brennan, G. J. Armstrong, J. Kelly and A. M. Whelan, *US Pat.* US 8,263,418 B2, 2012; (*b*) W. Zhang, X. Qiao and J. Chen, *Mater. Sci. Eng., B*, 2007, **142**, 1.